

# An Optically Coupled System for Quantitative Monitoring of MRI-Induced RF Currents Into Long Conductors

Marta G. Zanchi\*, *Student Member, IEEE*, Ross Venook, John M. Pauly, *Member, IEEE*, and Greig C. Scott

**Abstract**—The currents induced in long conductors such as guidewires by the radio-frequency (RF) field in magnetic resonance imaging (MRI) are responsible for potentially dangerous heating of surrounding media, such as tissue. This paper presents an optically coupled system with the potential to quantitatively measure the RF currents induced on these conductors. The system uses a self shielded toroid transducer and active circuitry to modulate a high speed light-emitting-diode transmitter. Plastic fiber guides the light to a photodiode receiver and transimpedance amplifier. System validation included a series of experiments with bare wires that compared wire tip heating by fluoroptic thermometers with the RF current sensor response. Validations were performed on a custom whole body 64 MHz birdcage test platform and on a 1.5 T MRI scanner. With this system, a variety of phenomena were demonstrated including cable trap current attenuation, lossy dielectric  $Q$ -spoiling and even transverse electromagnetic wave node patterns. This system should find applications in studies of MRI RF safety for interventional devices such as pacemaker leads, and guidewires. In particular, variations of this device could potentially act as a realtime safety monitor during MRI guided interventions.

**Index Terms**—Current sensing, heating, interventional devices, magnetic resonance imaging (MRI), safety.

## I. INTRODUCTION

MAGNETIC resonance imaging (MRI) employs high-power radio-frequency (RF) fields, which can induce currents in long conductors. For implanted devices, these RF currents can cause heating and pose safety risks in the clinical use of MRI [1], [2]. At present, the MRI community lacks reliable methods and systems to predict and monitor dangerous heating conditions.

The uncertainties of RF safety lead to the occurrence of unpredicted adverse events [3], [4], to the disqualification of entire patient populations from receiving any form of MRI scan if they have an implanted device (even in situations where it might be

safe), and to limitations in the development and use of interventional MRI devices [5], [6]. Our goals are to develop a sensor that can form the basis of an external guidewire RF monitoring system, and to create a research tool for study of induced currents on immersed wires and leads.

### A. Known Wire Current and Heating Behavior

Wire current and heating behavior has been studied by the MRI community since the first interventional devices were used with MRI. It is well known that conductive wires inside the electromagnetic field of an MRI bodycoil can behave like resonant linear dipole antennas [7]–[10]. This manifests as a substantial increase in the electrical energy stored by the wire in the form of large standing wave currents on the wire itself. Typically, when the wire end is placed in contact with a conductive medium, such as a saline solution, current flows into the medium, where we can observe dissipation of energy and the associated increase in the local temperature. RF heating is formally described by the bio-heat equation, given by

$$\rho c \frac{dT}{dt} = k \nabla^2 T + \frac{|J|^2}{\sigma} - h(T - T_o) \quad (1)$$

where  $h$  and baseline temperature  $T_o$  model perfusion,  $k$  is thermal conductivity,  $c$  is specific heat,  $\rho$  is tissue density and  $\sigma$  is electric conductivity. Neglecting perfusion, the steady state temperature depends quadratically on current density,  $J$ , i.e., both power density  $|J|^2/\sigma$  and  $T$ , will increase with the square of current density. The high electric field at the tip is commonly blamed for the heating, but of course, a high local current density must coexist in conductive solutions.

A systematic approach to the understanding of the distribution of current of the bare metal and insulated dipole embedded in a dissipative medium was pursued by King in the 1970s [11]–[16]. For the insulated dipole, the lossy media plays the role of the coax outer conductor. Following the notation used by King, the parameter most useful in the characterization of the dissipative medium is the complex wave number (or complex propagation constant)  $k$

$$k = \beta - j\alpha = \omega \sqrt{\mu \epsilon_e \cdot \left(1 - j \frac{\sigma_e}{\omega \epsilon_e}\right)} = \omega \sqrt{\mu \epsilon_e \cdot (1 - jp_e)} \quad (2)$$

where  $\beta$  and  $\alpha$  are the real phase constant and real attenuation constant, respectively, and  $p_e = \sigma_e/\omega \epsilon_e$  is the loss tangent. These parameters depend on the real permeability  $\mu$ , real effective dielectric constant  $\epsilon_e$ , and real effective conductivity  $\sigma_e$  of the medium, assumed here to be isotropic. The real phase

Manuscript received May 16, 2009; revised July 22, 2009; accepted August 25, 2009. First published September 15, 2009; current version published January 04, 2010. This work was supported by the National Institutes of Health under Grant R01EB008108, Grant R33CA118276, and Grant R21EB007715. *Asterisk indicates corresponding author.*

\*M. G. Zanchi is with the Electrical Engineering Department, Stanford University, Stanford, CA 94305 USA (e-mail: mgzanchi@stanford.edu).

J. M. Pauly and G. C. Scott are with the Electrical Engineering Department, Stanford University, Stanford, CA 94305 USA (e-mail: pauly@stanford.edu; greig@mrsrl.stanford.edu).

R. Venook is with Boston Scientific Neuromodulation, Valencia, CA 91355 USA (e-mail: ross.venook@gmail.com).

Color versions of one or more of the figures in this paper are available online at <http://ieeexplore.ieee.org>.

Digital Object Identifier 10.1109/TMI.2009.2031558

constant of the medium is of particular importance since it is inversely proportional to the characteristic wavelength  $\lambda = 2\pi/\beta$  of the RF field coupled to the wire embedded in the medium. Interestingly, as one progresses to higher fields, the loss tangent  $p_e$  decreases as dielectric effects on wave propagation become influential.

In the simple case of a straight, bare wire parallel to the symmetry axis of the MRI scanner, the conditions for resonance and the generation of a transverse electromagnetic (TEM) field are established when the wire length  $L$  is an integer number of half the wavelength of the dissipative medium. Embedded in air, the bare, straight wire has a  $\sim 230$  cm minimum resonant length at 64.0 MHz; embedded in tissue ( $\sigma \sim 0.5$ ,  $\epsilon_m \sim 80\epsilon_0$ , so  $\beta \sim 14.7$ ), it has a minimum resonant length of  $\sim 21$  cm at that same frequency.

In reality, the situation of a straight, bare wire in a completely homogenous, isotropic medium is not a realistic representation of situations commonly encountered in an MRI scanner. Typically, the wire construction and the nature of its environment can change the value of  $\lambda$  significantly, making the task to predict potentially dangerous resonant conditions very difficult. For example, the thickness and dielectric constant of wire insulation effectively increases the wavelength, while coiling can cause a physically short wire to resonate at lower frequencies. Within an MRI scanner, a circularly polarized birdcage coil generates an electric field component parallel to  $B_0$  that, ideally, increases linearly with the radial distance from the center of the coil, but in reality, diverges from linearity near the endrings and near the bodycoil shield. The quasi-linear increase of the RF field with the radial distance is expected to create a proportionally increasing RF current in a wire held parallel to the coil axis, and an associated quadratic increase in the temperature rise at the wire end embedded in a conductive medium. Given some knowledge of the expected geometrical tissue-wire interface, a quantitative measure of the driving current is a prerequisite if one is to detect and prevent dangerous heating conditions.

Many devices and wire constructions have been proposed to prevent wire resonance and heating, but with limited effectiveness. At the free-end of a wire, where  $E$  fields are maximum and energy storage is primarily capacitive, one can deliberately couple by immersion to a lossy dielectric, thereby spoiling the quality factor of the resonant wire [17]. More commonly, cable trap devices prevent dangerous heating conditions by targeting regions of high RF current, where energy storage is inductive. Toroidal cable traps inductively couple a high resistance in series with the wire to spoil the resonant  $Q$  or modify the resonant frequency of the wire. Here, the wire itself acts as the primary coil, and a resonant toroidal cavity enfolding the wire acts as the secondary coil. In 2000, Ladd and Quick [18] added coaxial chokes with length  $\lambda/4$  to coaxial cables in order to reduce the amplitude of the MRI-induced currents on the cable shields. In 2005, Hillenbrand *et al.* [19] described the “bazooka coil,” a balun-style RF trap, and demonstrated its capability to reduce the formation of resonating RF waves on long conductors during transmission [15]. Hillenbrand also interfaced the cable trap to a preamplifier circuit, used in this case as a dual-mode receiver. For maximum attenuation effectiveness, the location of the current maxima has to be known *a priori*.

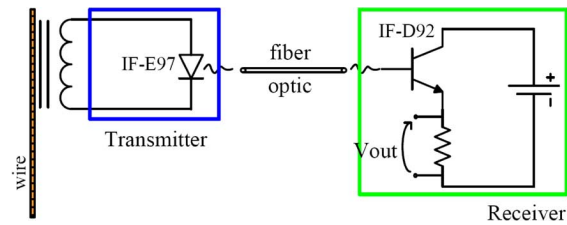


Fig. 1. Simplified block diagrams of the early prototype RF current monitoring system.

## B. Early Prototypes

Our early work focused on an optically coupled guidewire sensor [20]–[25]. Fig. 1 illustrates the archetype of this RF current monitoring system, developed by Venook *et al.* [17]. It consisted of an 11-turn, air-core, 1.50 cm toroidal transformer in which the guidewire acted as the primary, and the toroid as the secondary. The toroid output voltage was half-wave rectified by an Industrial Fiber Optics IF-E97 light-emitting-diode (LED). For RF voltage thresholds exceeding approximately 1.9 V, the resulting dc current self-biased the LED, whose light output in turn biased an IF-D92 high-sensitivity NPN phototransistor receiver via a 1000  $\mu\text{m}$  core polymethyl-methacrylate (PMMA) plastic optic fiber. In its common collector configuration, the phototransistor emitter resistor (1.2 K $\Omega$ ) developed an output voltage proportional to the rectified guidewire RF current. This simple system preserved the electrical continuity of the wire, while the optical transmission eliminated all electromagnetic interactions that are problematic for coax cables. However, the LED device nonlinearity at the turn-on threshold limited its utility for measuring low level signals where the threshold capacitance and RF impedance swing presented a nonlinear load to the toroid. This limitation made the system difficult to characterize and use.

## C. Goals of the New Current Monitor

To overcome these uncertainties, we have designed and built an optically coupled system that independently and quantitatively detects RF currents in long conductors, such as wires and leads of medical or interventional devices. We have conducted a series of experiments to test the capability of our RF monitoring system to measure the currents induced in bare wires by MRI in a variety of conditions, differing by the wire length or position, the bodycoil excitation, and the use of gelled or non-gelled saline solution at the wire end. In most of these experiments, we have simultaneously recorded the temperature rise associated with these currents at the wire end. We have validated our findings against the known wire current and heating behavior. We have also used the RF monitoring system and temperature measurements to assess the capability of cable-traps and  $Q$ -spoiling loads to reduce the RF currents and heating at or near resonant conditions. Finally, we have studied the pattern of the RF currents along the embedded bare wire and compared our findings against the present understanding of transverse electromagnetic (TEM) wave propagation. In the remainder of this paper, we introduce our RF current monitoring system and a series of methods and experiments that validate this system against the known wire current and heating behavior.

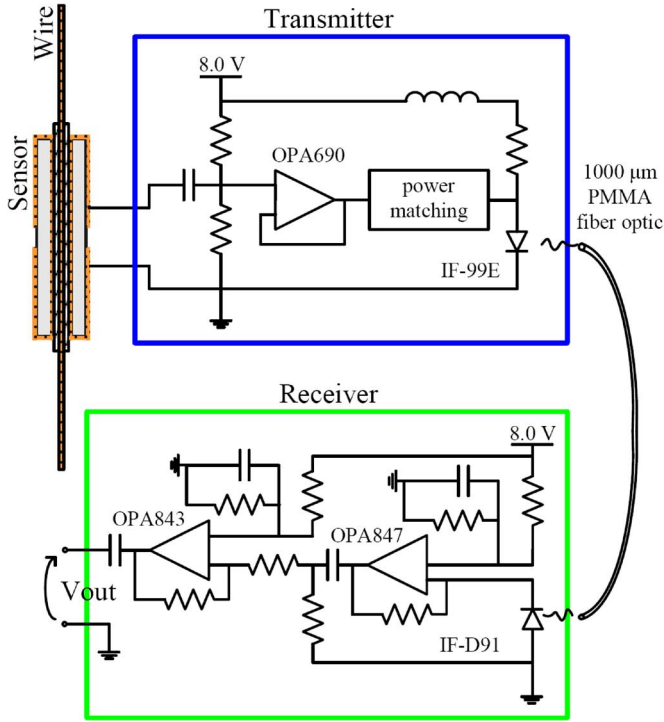


Fig. 2. Simplified block diagrams of the new RF current monitoring system.

## II. THEORY OF OPERATION

To overcome the limitations of the early prototype RF monitoring system, we recently developed a new version, incorporating a self-shielded toroid cavity with active circuitry in both the transmitting and receiving circuits. Fig. 2 illustrates the schematic of our newly developed RF current monitoring system, designed and dimensioned for operation near 64.0 MHz, that is, at the Larmor frequency of a 1.5 T scanner.

The toroid-cavity acts as a volume-rotated rectangular single turn transformer secondary, that is, a rectangular single turn transformer secondary rotated  $360^\circ$  around the cylindrical axis. It consists of copper tape wrapped around a toroidal Teflon core with 1.55 mm inner diameter and 5.50 mm outer diameter. Any long conductor fed through the core of the toroid acts as the transformer primary. MRI-induced currents on the wire, will couple a magnetic flux to the toroid secondary given by

$$\Phi = \int_a^b \frac{\mu_0}{2\pi \cdot r} g \cdot I \cdot dr = \mu_0 \cdot \frac{\ln(\frac{b}{a})}{2\pi} \cdot g \cdot I = MI \quad (3)$$

where  $a$ ,  $b$  are the inner and outer radius of the toroid, respectively;  $g$  is the length of the toroidal cavity;  $I$  is the wire current, and  $M$  is mutual inductance. Faraday's law yields the toroid voltage

$$V = M \cdot \frac{dI}{dt} \quad (4)$$

To determine overall circuit performance, the toroid impedance parameters (inductance  $L$  and series resistance  $R_T$ ) are also useful and are again a function of geometry via

$$L = \mu_0 \cdot \frac{\ln(\frac{b}{a})}{2\pi} \cdot g \quad (5)$$

$$R_T = \left(\frac{g}{a} + \frac{g}{b}\right) \cdot \sqrt{\frac{\mu_0 \cdot f_{RF}}{4\pi \cdot \sigma}} \quad (6)$$

where  $\sigma$  is the conductivity of the copper tape ( $5.8 \cdot 10^7$  S/m); and  $f_{RF}$  is the frequency of the bodycoil excitation coupling to the wire. The toroid is terminated in a  $500\text{-}\Omega$  load, which will reflect a negligible series resistance back to the wire. This is in contrast to the cable trap case, where, defining the quality factor,  $Q_T = 2\pi f_{RF} L / R_T$ , and noting that  $L = M$ , the series impedance induced at the wire has an upper limit of

$$\Delta Z \approx (2\pi f_{RF})^2 \cdot \frac{L^2}{R_T} = Q_T^2 \cdot R_T \quad (7)$$

when capacitors resonate with the toroid to create high blocking impedances. As a sensor, the toroid system must minimally disturb the guidewire behavior.

For the transmitter, the toroid-cavity is connected via a 2.2 nF capacitance (chosen for series resonance hence minimum impedance) to the noninverting input of an OPA690 operational amplifier in unity-gain buffer configuration. This input is biased at half the supply voltage by two 1 K $\Omega$  biasing resistors which in turn present a  $500\text{-}\Omega$  RF termination to the toroid. The OPA690 is power-matched at its output to a low-cost IF-E99 LED biased through a bias-tee. This LED is specified for 150 MB/s data rates. At 8.0 V supply voltage, the transmitter has an overall standby current consumption of less than 30 mA, 10 mA of which is the dc biasing current of the LED. Although this device is intended to monitor wire current exterior to the imaging volume, current carrying wires are twisted to prevent a net field distortion in the unlikely event of imaging at the device location. At the 8.0 V supply voltage, the LED and bias-tee (3.7  $\mu$ H choke with a 637- $\Omega$  series resistance) have an overall reactance of  $j16.5 \Omega$  at 64.0 MHz, which has been matched to the output of the OPA690 via a series 150 pF ( $-j16.5 \Omega$  at 64.0 MHz) capacitor. The output is impedance-matched to the LED such that, to a first approximation, the LED current and light intensity are linearly proportional to the toroid signal. The LED light output is sent via a 1000  $\mu$ m core PMMA plastic optic fiber to the photonic receiver end of the RF monitoring system.

In our prototype, the transmitter is powered by stacking three Duracell DL2450 lithium batteries, each of nominal voltage 2.7 V when loaded (3 V unloaded). This lightweight battery provided about 540 mAh capacity, allowing up to 3 h of reliable safety monitoring, and has been used safely in a 1.5 T field.

At the receiver, the RF modulation of the LED light output is restored to an RF voltage by a low-cost IF-D91 photodiode (PD) connected to a two-stage amplifier employing an OPA847 and an OPA843. The first stage is a low-noise transimpedance amplifier of maximum gain 10 K $\Omega$  (to ensure stability at 64.0 MHz). The second stage receiver amplifier is an inverting voltage amplifier. The OPA843 has nominal, minimum GBP of 558 MHz and minimum noise gain of 3; thus it can be operated in an inverting amplifier configuration with a gain in the range 2.0–8.7 V/V at 64.0 MHz.

## III. METHODS

To monitor a wide range of RF wire currents associated with different heating conditions, we employed different combina-

TABLE I  
GEOMETRY OF TOROIDAL SENSORS

Toroid Type	Length	Diameter
	[mm]	[mm]
TA	20	7
TB	27	7
TC	57	6

Length and diameter of the three available toroidal sensors.

TABLE II  
COMPARISON OF GAIN OF CURRENT MONITORING SYSTEMS

System Configuration	Toroid Type	Receiver Transimpedance Amplifier Gain	Total Gain	Relative Gain
		[K $\Omega$ ]	[V/A]	
TA-GL	TA	20	1.50	0.17
TA-GH	TA	80	6.10	0.68
TB-GL	TB	20	1.12	0.12
TB-GH	TB	80	4.50	0.50
TC-GL	TC	20	2.25	0.25
TC-GH	TC	80	9.00	1.00

Measured gain ( $V_{OUT}/I_{WIRE}$ ) of the receiver two-stage transimpedance amplifiers, as well as of the overall RF monitoring systems obtained with several combinations of coils and receivers. The receiver transimpedance amplifier is the two-stage amplifier after the IF-D91 photodiode.

tions of sensors and receivers with different sensitivity and gain, respectively.

Specifically, we have implemented two versions of the same receiver, differing by only the gain of the two-stage transimpedance amplifier. The transimpedance amplifier of the highest-gain (GH) receiver has nearly the maximum value to ensure stability (80 K $\Omega$ ). The lowest-gain (GL) receiver has about 25% the overall gain of the former (20 K $\Omega$ ).

In addition, during our experiments we have employed three toroids of different sensitivity, which we can vary by modifying the toroid's length or diameter. We refer to the three toroids as TA, TB, and TC, respectively; their dimensions are shown in Table I.

We calibrated the RF current monitoring system on the test bench by applying a 64.0 MHz, 200 mA<sub>pp</sub> current from an Agilent 33250A waveform generator (10 V<sub>pp</sub> max voltage, 50- $\Omega$  output impedance) into a wire fed through the transmitter toroid. Table II lists the overall gains (in  $V_{out}/I_{wire}$ ) of the RF monitoring system obtained with various combinations of coil (TA, TB, or TC) and receiver (GH or GL). During the experiments described in this paper, we used the combinations with lowest overall gain (TA-GL, TB-GL) in high RF current conditions, and the combinations with highest overall gain (TA-GH, TB-GH, TC-GH) in low RF current conditions.

To perform all but one of our experiments, we used an RF safety test platform composed of a shielded 8-rung birdcage that was previously constructed at Boston Scientific Scimed in Maple Grove Minnesota. The birdcage RF safety test platform replicates the field (and, heating) patterns seen within an MRI

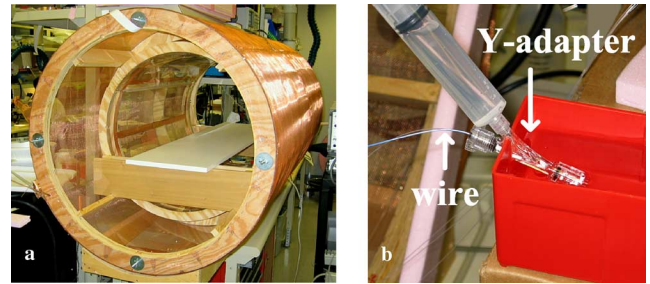


Fig. 3. Birdcage (a) and close-up of the catheter Y-adapter in saline bath (b).

scanner to study the resonance properties of guidewires at a comparatively negligible fraction of the cost of a complete MRI system and without the need to face the challenges posed by the static magnetic field during the initial stage of developing new safety devices. The birdcage was 100 cm long, 60 cm diameter and was inserted in a 150 cm long shield of 82 cm diameter. End-ring capacitors were 66 pF, while each leg rung required three capacitor segments: the outer two were 18 pF and the middle was 22 pF. The birdcage was a hybrid design since it had capacitors in the rungs and endrings. However, aside from the end-ring resonance (at the lowest frequency), the modes exhibited a low-pass behavior, in which the lowest frequency birdcage mode was the uniform field mode, and the other resonant modes created various gradient and higher spatially inhomogeneous field patterns. In these tests, the birdcage was linearly polarized; consequently, wires were placed in a plane orthogonal to  $B_1$  where  $E$  fields will be maximum. The RF safety platform is controlled by an Agilent 33250A waveform generator and a Kalmus model KAA2040M2 1–100 MHz, 200 W power amplifier. We operated the birdcage RF safety platform by driving the RF power amplifier with a sinusoid at the resonant frequency of 64.0 MHz. The sinusoid was modulated by 5 ms rectangular pulses at 10 ms TR. The duty cycle was 50%. The RF power varied from 3.5 to 55 W, depending on the experiment conditions. Even at these power levels, with light loading, this birdcage could still create RF electromagnetic fields and heating comparable to that of an MRI scanner. Under a 100 Kg load, a continuous 200 W excitation—neglecting radiation and coil losses, as is standard—should still be able to produce 2 W/Kg SAR, comparable to many MRI sequences.

In most of our experiments, we placed a 22 AWG copper wire of various lengths parallel to the center axis (the  $z$ -axis) of the birdcage, at known radial distance from the latter. The tip of the wire was fixed at 25 cm before the opening of the birdcage. To measure the temperature increase at the wire tip, we secured the fiber-optic temperature sensor of a Luxtron m3300 Biomedical Lab Kit within 1 mm from the tip of the wire and placed both into a catheter Y-adapter to create a repeatable but constrained heating area with access to a small 0.5 M saline bath. To measure the wire current, the RF monitoring system of fixed overall gain, depending on the chosen toroidal sensor and amplifier gain, was placed at a known distance from the tip of the wire. Fig. 3 shows the 8-rung birdcage (a) and a close-up of the catheter Y-adapter in the saline bath (b). Fig. 4 schematically illustrates the typical setup of our experiments. As a sanity test, we measured heating for a 170 cm wire with no sensor, and with a sensor placed at

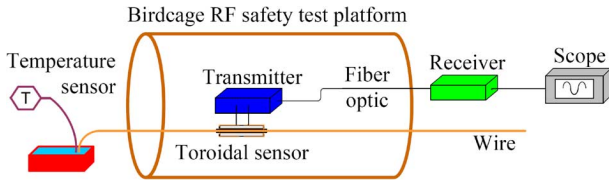


Fig. 4. Typical experimental setup.

three different locations on the wire. For all cases, we achieved the same  $25\text{ }^{\circ}\text{C}$  rise ( $\pm 1\text{ }^{\circ}\text{C}$ ). We concluded that the sensor was creating only minor perturbations in the induced RF current on the wire.

Using these methods (or slight variations of the same, which will be discussed), we validated our sensor in a series of five experiments that investigated: 1) the resonant wire length and dielectric  $Q$ -spoiling method; 2) the cable trap  $Q$ -spoiling method; 3) the wire current position dependency; 4) the use of a gelled phantom; and 5) the TEM wave effects in water. In a sixth experiment, we replicated our test method to search for the resonant wire length in a 1.5 T MRI system.

#### IV. EXPERIMENTS AND RESULTS

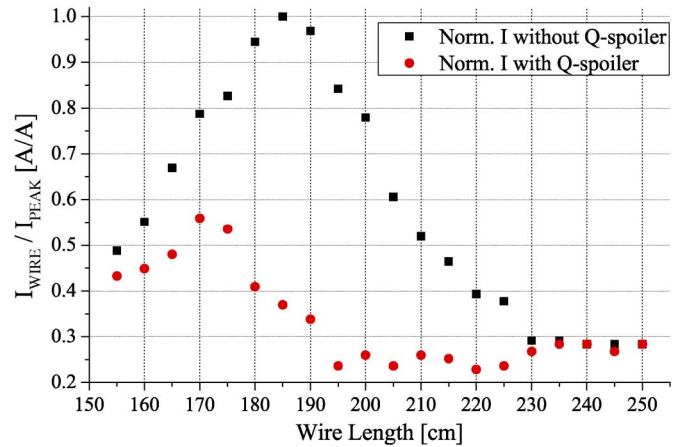
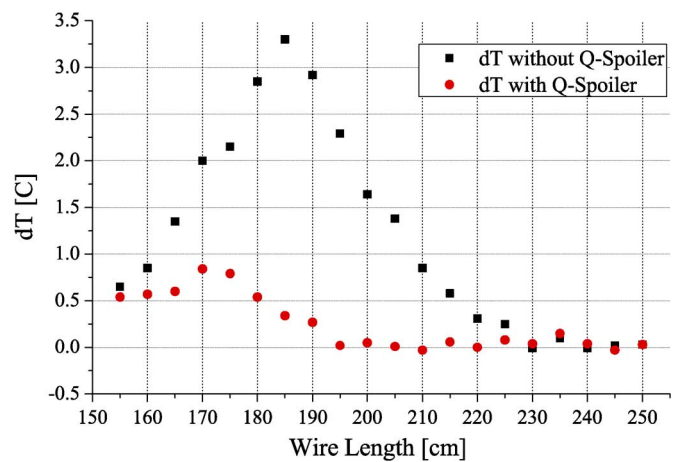
##### A. Resonant Wire Length and Dielectric $Q$ -Spoiling Method

In the first experiment, we used our RF current monitoring system to investigate the resonant length of the bare wire and to determine whether a simple lossy device connected to one of the wire ends will substantially reduce the RF currents at several wire lengths; we assessed our results against those obtained by simultaneously measuring the heating at the other wire end.

The RF monitoring system had configuration TB-GH, and was placed 60 cm from the tip of the wire, where the Luxtron temperature sensor had been secured. At the opposite end of the wire, we prepared a plastic bottle containing 0.4 l of a 2 M saline solution, acting as a lossy dielectric load. We fed a 5 cm long copper lead through a small hole in the top of the bottle; 1 cm of the lead was outside the bottle and soldered to a small copper alligator clip, which could clamp to the wire under test. The wire was placed 15 cm radially from the symmetry axis of the birdcage.

Starting from a wire length of 250 cm, we measured the RF current and temperature rise first by loading the wire with the 2 M saline lossy load; then, without loading it. We repeated this procedure 20 times, each time after cutting 5 cm off the total wire length. Between steps, we flushed the syringe until temperature returned to equilibrium.

Figs. 5 and 6 compare the sensor output measured by our system with the temperature rise, with and without the lossy dielectric at the wire end. In both cases, we observe that for each increase (or, decrease) in the measured heating for the progressively shorter wire, there is a simultaneous increase (or, decrease) in the current magnitude. In the absence of the 2 M saline solution, the wire current and temperature rise peaked at a 185 cm wire length (the peak value of wire current was, in this case,  $95\text{ mA}_{\text{RMS}}$ ), whereas when the wire was electrically connected to the lossy load, the RF current and temperature peaked at 170 cm, yet created only a quarter of the prior heat increase.

Fig. 5. Normalized wire currents, with and without dielectric  $Q$ -spoiler, at several lengths of the copper wire. We estimated  $I_{\text{PEAK}}$  to be  $95\text{ mA}_{\text{RMS}}$ .Fig. 6. Temperature rise, with and without dielectric  $Q$ -spoiler, at several lengths of the copper wire.

##### B. Cable Trap Spoiling Method

In a second experiment, we used the RF current monitoring system to measure the effect of a custom-made cable trap on a near-resonant wire at several values of bodycoil excitation, and compared our results against those obtained by simultaneously measuring the heating at the wire end.

The RF monitoring system had configuration TA-GH and was placed at 60 cm from the tip of the wire. The near-resonant (180 cm long) copper wire was placed 5 cm radially from the symmetry axis of the birdcage. The custom-made trap, displaced 20 cm from the RF monitoring system, had inner radius  $b = 8.17\text{ mm}$ , outer radius  $a = 1.55\text{ mm}$ , and length  $g = 26.31\text{ mm}$ , where “inner radius” is that of the hollow copper foil tube through which the wire is fed and “outer radius” is the outside toroid foil dimension. The ideal, calculated  $L$ ,  $R_T$ , and  $Q_T$  of this trap were 8.77 nH, 6.70 m $\Omega$ , and 527, respectively. The ideal estimated series blocking impedance was 1.8 K $\Omega$ , the measured blocking impedance was nearly 600  $\Omega$ , and the difference between the two was mainly due to the lower effective  $Q_T$  (300, measured).

We sensed the RF wire current and the temperature rise at the wire tip for birdcage RF power levels increasing progressively from 4.5 to 39.5 W. Then we removed the RF trap and repeated the experiment.

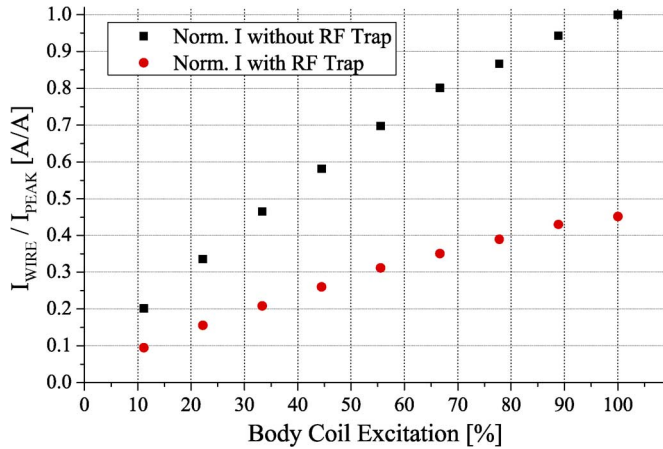


Fig. 7. Normalized wire currents, with and without RF trap, at increasing bodycoil excitation. We estimated  $I_{PEAK}$  to be  $100 \text{ mA}_{\text{rms}}$ . The maximum body coil excitation is  $39.5 \text{ W}$ .

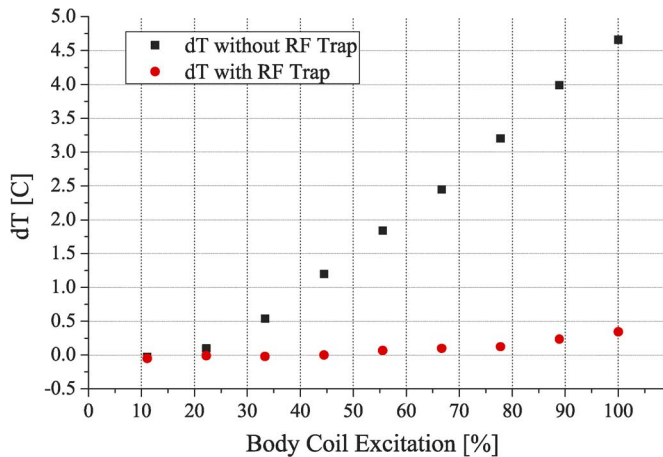


Fig. 8. Temperature rise, with and without RF trap, at increasing bodycoil excitation. The maximum body coil excitation is  $39.5 \text{ W}$ .

Figs. 7 and 8 compare the sensor response measured by our system with the temperature rise, with and without the cable trap. In both cases, the wire current and temperature increase with the bodycoil excitation, but the amplifier appears to exhibit a weak nonlinearity at the higher power levels. The temperature increased approximately with the square of wire current without the trap. With the trap present, the temperature increase was too small to reliably show the quadratic dependence. The maximum value of wire current, measured without RF trap at maximum body coil excitation, was  $100 \text{ mA}_{\text{rms}}$ .

### C. Position Dependency

In a third experiment, we tested our RF monitoring system against our knowledge of the RF field pattern in the bodycoil and against the measured temperature rise at the tip of a resonant wire [26]–[28].

The RF monitoring system had configuration TB-GL and was placed at  $40 \text{ cm}$  from the tip of the wire. The resonant ( $185 \text{ cm}$  long) copper wire was initially placed along the symmetry axis of the birdcage; at each step of the experiment, we increased its radial distance by  $20 \text{ mm}$  and recorded both the wire current and the temperature rise at the wire tip.

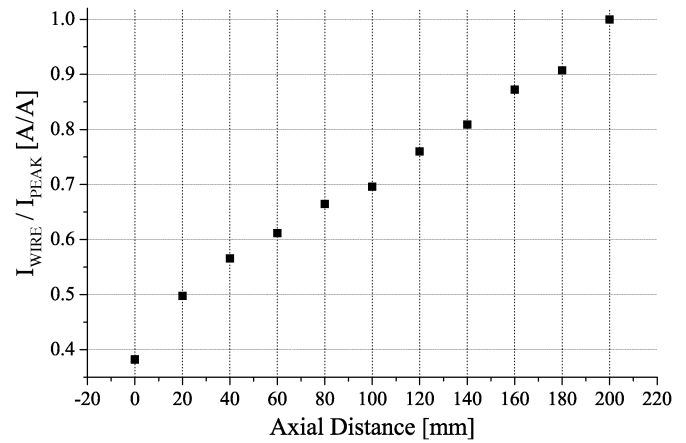


Fig. 9. Normalized wire currents at increasing radial distance from the symmetry axis of the birdcage. We estimated  $I_{PEAK}$  to be  $320 \text{ mA}_{\text{rms}}$ .

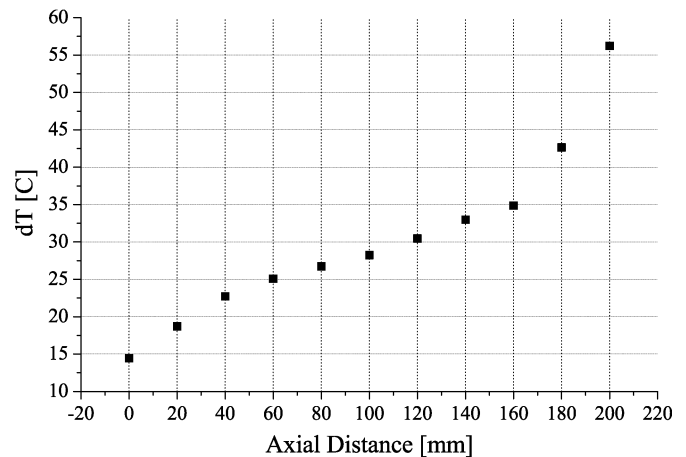


Fig. 10. Temperature rise at increasing radial distance from the symmetry axis of the birdcage.

The sensor response in Fig. 9 show that, in the range of radial distance from  $40$  to  $160 \text{ mm}$ , the increase of the measured wire current is linear to a good approximation, and the corresponding increase of the measured heating at the wire end (in Fig. 10) goes approximately with the square of current. The maximum value of wire current, measured at  $200 \text{ mm}$  from the center of the body coil, was  $320 \text{ mA}_{\text{rms}}$ . Unlike ideal infinitely long birdcages, end-ring E fields and rung capacitors E fields are significant in practical resonators. Near the symmetry axis of the birdcage, as well as near the outer shield of the birdcage, both the wire current and heating diverge from their linear and quadratic behavior, respectively; yet, in these conditions, the measured increase in the temperature is consistent with (i.e., depends quadratically on) the measured increase in the RF current.

### D. Validation in Gelled Saline Phantom

In a fourth experiment, we tested the capability of our RF monitoring system to operate on a resonant wire even when immersed in a phantom mimicking the characteristics of tissue. We tested the measured wire currents against the temperature rise at the wire tip.

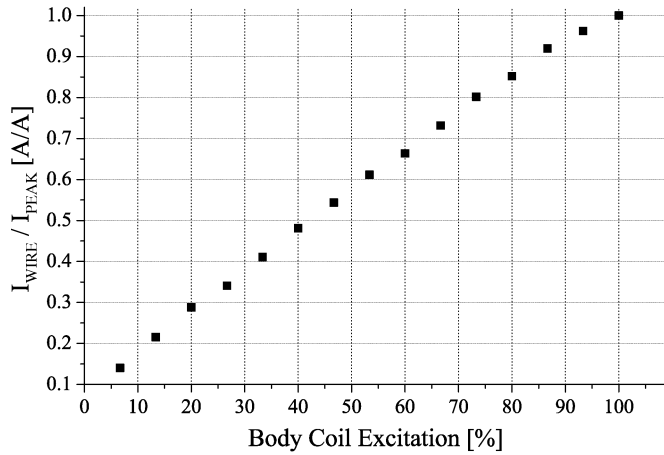


Fig. 11. Normalized wire currents with increasing bodycoil excitation. The wire is partially submerged in a gelled phantom. The maximum body coil excitation is 52.5 W. We estimated  $I_{PEAK}$  to be  $390 \text{ mA}_{\text{RMS}}$ .

Park *et al.* [29] have shown that evaluation of MR-induced heating in a medical device should be performed with phantoms with shape and composition simulating the environment that the device experiences in the body. The phantom should have high enough viscosity to avoid thermal convection where the heating is measured; and it should simulate the conductivity of tissue (0.25 S/m). We prepared a gelled phantom that had both these characteristics by adding 32.80 g of Polyacrylic acid by Sigma–Aldrich and 2.87 g of NaCl to 4.1 l of distilled water, in a  $23.0 \times 35.0 \times 12.5 \text{ cm}$  plastic container. A portion of a resonant wire was submerged in the gelled phantom (185 cm overall wire length, 45 cm submerged) and isolated by means of a shrinkable tube, except for a small area of 1 cm near the tip. The remaining length of the wire was placed at 14 cm axial distance from the symmetry axis of the birdcage.

We encapsulated the transmitter and its battery in a waterproof cylindrical plastic case (9 cm diameter, 2 cm height), and submerged it in the gelled phantom. The toroidal sensor was left outside the case, at 25 cm from the tip of the wire, and connected to the transmitter via a pair of twisted leads (8 cm) fed through a small, waterproof hole in the side of the case. The RF monitoring system had configuration TB-GL. We simultaneously monitored the RF wire current amplitude and temperature rise at the tip of the wire while increasing the bodycoil excitation, from 3.5 to 52.5 W in steps of 3.5 W. To ensure close contact between the thermometer and the wire tip, we attached the sensitive part of the fiber-optic sensor (4 mm long, at 5 mm from the fiber tip) to the bare wire tip using a small piece of copper tape.

Figs. 11 and 12 show the sensor response and temperature rise, respectively, with increasing bodycoil excitation. The temperature rise increased quadratically with respect to the wire current. The maximum value of wire current, measured at maximum body coil excitation, was  $390 \text{ mA}_{\text{RMS}}$ .

#### E. TEM Wavelength in Water

In a fifth experiment, we measured the wire current profile along a bare, submerged wire and validated our findings against the theoretical analysis by King *et al.* [11]–[16].

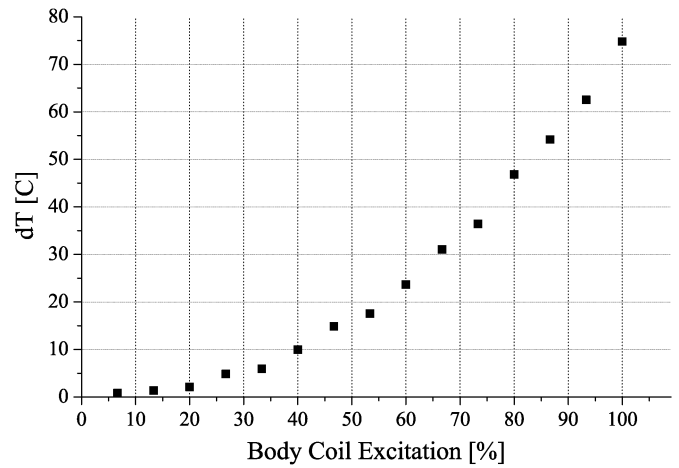


Fig. 12. Temperature rise with increasing bodycoil excitation. The wire is partially submerged in a gelled phantom. The maximum body coil excitation is 52.5 W.

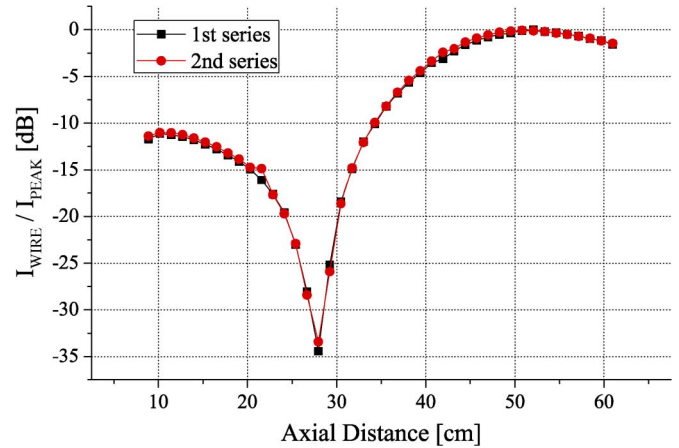


Fig. 13. Normalized wire currents at different positions along the length of a bare copper wire immersed in water. We estimated  $I_{PEAK}$  to be as low as  $1 \text{ mA}_{\text{RMS}}$ .

We placed a bare copper wire, of length 150 cm, in an oblong open tank filled with 4.5 l of distilled water. We secured our RF monitoring system on a lightweight movable cart made of expanded polystyrene, which could be slid continuously along the edge of the open tank. The toroidal sensor, perpendicular to the plane of the cart, was immersed in the water, where it enclosed the wire.

The open tank was positioned inside our birdcage RF safety test platform, its long axis parallel to the  $z$ -axis of the birdcage, at 10 cm radial offset from the center.

We operated the birdcage RF safety platform at a power of 40 W. We measured the wire current at several positions of the toroidal sensor along the length of the wire, starting at 9 cm from the end of the wire and moving in steps of 1.3 cm up to a distance of 61 cm. Given the low amplitude of the measured points, we used the swept spectrum function of a HP 3589A Analyzer to measure the receiver output voltage.

The points in Fig. 13 are the RF sensor response measured by our monitoring system at the different positions along the length of the bare copper wire. This figure presents the results of two different series of measurements. The profile of the RF

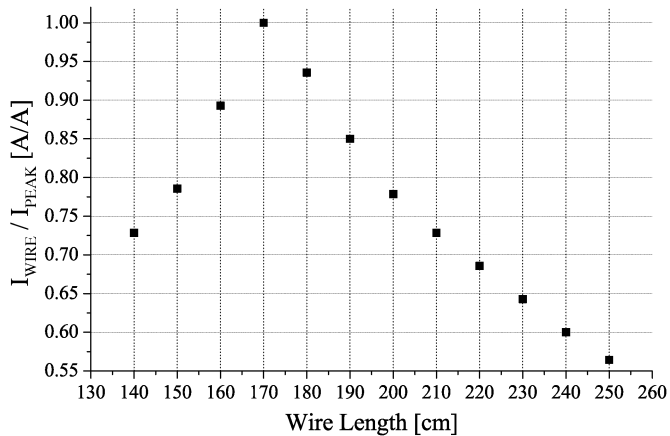


Fig. 14. Normalized wire currents at several lengths of the copper wire in a 1.5 T scanner. We estimated  $I_{\text{PEAK}}$  to be  $80 \text{ mA}_{\text{rms}}$ .

current magnitude on the bare wire is characterized by maxima separated by a distance  $\lambda$  equal to 43 cm. The maximum value of measured wire current was very low ( $1 \text{ mA}_{\text{rms}}$ ).

#### F. Validation in 1.5 T

Ultimately, the RF safety monitoring system is intended to operate in an MRI scanner during imaging procedures. The main differences between the MRI environment and the birdcage RF safety test platform are the presence of a strong static magnetic field and pulsed gradient fields. The static field could apply translational and rotational forces on magnetic objects, while the latter applies a time-varying magnetic flux and thus induces currents. To ensure that the operation of the RF current monitoring system is not affected by either the static field or the pulsed gradient field, we have replicated our standard heat test setup to search the resonant length of the bare wire inside an MRI scanner.

We placed a bare copper wire parallel to the  $z$ -axis of the scanner. The initial wire length was 250 cm. One end of the wire was fixed onto the MRI bed at the head-side opening of the MR bore, at 10 cm from both the  $x$ ,  $y$  axes. At the opposite end of the wire, we cut the wire in lengths ranging from 250 cm to 140 cm in 10 cm decrements. We placed the RF monitoring system at the foot-side opening of the MR bore and secured it on the bed with standard adhesive tape.

The magnetic resonance procedure was performed with a 1.5 T Signa MR scanner. The imaging pulse sequence was a standard 3-D gradient recalled echo (GRE) sequence. The repetition period (TR) was 40 ms and the total scan time 3.08 s.

The points in Fig. 14 are the measured responses of our RF monitoring system. The maximum RF current was  $80 \text{ mA}_{\text{rms}}$  and occurred at the wire length of 170 cm. The difference in dimensions between a clinical birdcage and our test system will influence the wire length for maximum current because the coupled volume will change. Even so, typical guidewire dimensions of 145–180 cm fall within the peak heating lengths.

## V. DISCUSSION

Our experiments confirm that the amplitude of the RF voltages produced by our newly developed system provides a quantitative measure of the relative wire current amplitudes, and thus

of the potential for dangerous heating conditions when the wire is embedded in part in a conductive medium. In initial tests with the sensor inserted or removed we observed comparable heating behavior, suggesting that induced currents in wires undergo only minor perturbations in the presence of the measurement device. Unlike the cable trap receiver of Hillenbrand [19], which inserted a high impedance, our device was untuned and unable to inductively insert significant impedance changes. This was consistent with the similarity of result in heat measurements lacking this transducer.

We have demonstrated that a lossy dielectric attached to the end of the wire acts as a  $Q$ -spoiling device (experiment 1). In particular, at the resonant length, the 0.4 l  $Q$ -spoiler reduced the RF power of the guidewire current to  $<14\%$  of its value in the free wire. We have also demonstrated (experiment 2) a tuned cable trap that reduced the current sensor response for the near-resonant wire current to less than 50% of its value in the free wire for any level of intensity of the RF power driving the birdcage. However, the heating dropped a factor of 10. We believe that the trap location caused the sensor to be located nearer the maximum of a much lower wave amplitude on the wire, whereas without the trap, the sensor was further from the much large wave amplitude maxima. Consequently the heat and sensor readings do not scale. These conclusions are supported by both the increase in the amplitude of the wire currents measured by our current monitoring system and the temperature rise detected by the commercially available Luxtron thermometer.

We have also demonstrated that our system is a promising solution for RF safety monitoring even in situations where the toroidal sensor has to be submerged in a gelled phantom for evaluation of MR-induced heating in an environment simulating the viscosity and conductivity of tissue. In experiment 4, the wire current amplitude increases steadily with the bodycoil excitation even if the toroidal sensor is in contact with the gel. It is worth noting that, in this experiment, we changed the position of the toroidal sensor along the wire from 60 cm (in experiments 1 and 2) to 25 cm, measured from the wire tip. This difference changes the ratio of the wire current to the temperature rise compared to the first two experiments. It is also worth noting that the end part of the wire was, in this experiment, slightly bent, and yet the monitoring system worked properly as validated by the simultaneous measurement of heating.

Ultimately at least two sensors may be needed to capture the wave amplitude properties on a wire. Indeed, we know that the current profile in the resonant wire is characterized by maxima and minima. We have used our current monitoring system to measure the actual profile of the current into a bare wire immersed in water. Moreover cable trap placement could shift node maxima, while coiling and transitions from air to embedded tissue will also change boundary conditions for current distribution along a wire. Rather than attempting to pinpoint a single maxima, we anticipate that at least two sensors strategically separated (say by a quarter wavelength) in air could capture wave behavior. Variations of this approach will be needed for robust real-time safety monitoring of wires.

In experiment 5, the measured profile is characterized by maxima separated by a distance  $\lambda$  equal to 43 cm. This result is corroborated by the analysis of King *et al.* [11]–[16].

According to King's analysis in the case of pure distilled water at 15 °C as the embedding medium ( $\lambda = 1.26 \mu\text{N}/\text{A}^2$ ,  $\epsilon_e = \epsilon_e \cdot \epsilon_0 = 88 \cdot \epsilon_0$ ,  $\sigma = 5.5 \mu\text{S}/\text{m}$ ) and at the birdcage resonant frequency, the loss tangent  $\text{pe}$  and real phase constant  $\beta$  are, respectively,  $1.73 \cdot 10^{-5}$  and 12.8 rad/m, and the characteristic wavelength  $\lambda$  is, therefore, equal to 49 cm. The measured wavelength thus differs by only 6 cm from the theoretical value predicted by King's analysis of the properties of the bare wire embedded in distilled water (assumed by King to be an infinite, homogenous and isotropic medium, an idealization that can be accounted for the discrepancy between the measured and calculated result).

Finally, we have also validated our system by searching for the resonant length of the bare wire in a 1.5 T scanner. The successful outcome of this experiment demonstrates that the RF monitoring system is not affected by the static magnetic field and pulsed gradient fields of a clinical MRI scanner and thus can be safely and reliably used in a clinical scanner during an imaging procedure. We expected and interpreted the difference in the wire resonant length between the birdcage (185 cm) and the scanner (170 cm) as a consequence of the asymmetric wire placement in the scanner, the  $E$  field end ring patterns, and the different bodycoil length that changes the coupled volume. While we have not tested the monitoring system in the scanner using MR pulse sequences other than a 3-D GRE, the wide bandwidth and high speed of operation of our device—demonstrated on the bench—allows measuring the currents induced by substantially all clinical sequences used at 1.5 T.

As discussed throughout this paper, other strengths of our current measurements system are: it is able to probe currents along the wire, without the need to interrupt its continuity; it eliminates common mode RF coupling; it need not be in the imaging volume; and, it can monitor currents in real time.

These strengths represent significant advantages over alternative potential methods of current monitoring such as classic current transducers and standard pickup loops. Classic current transducers are ferrite toroids which saturate in the MRI field, creating inhomogeneity and forces. Standard pickup loops are sensitive to the body coil B1 field; in addition, narrow band baluns are needed to inhibit the coaxial signal return that tends to support common mode RF signal, which in turn distorts the local RF fields. B1 mapping methods are a new and very promising way of measuring wire currents but they work only in the region being imaged [30], [31]; we believe that the current monitoring system we propose in this paper could be used, in the future, to validate these emerging mapping techniques.

One limitation of our present design is that, despite the absence of coax cable, it is not fully balanced and it is thus susceptible to the electric field from the wire and possibly birdcage. To first order, the radial electric field component of a wire increases linearly along the wire, away from the current maxima. Its influence can be detected by first observing the output of the monitoring system when the toroidal sensor is placed next to the wire in the working bodycoil, and comparing this output to the measured wire current in the same experimental conditions. Second, the toroid orientation on the wire can be reversed and outputs compared. Asymmetric shielding, sensor construction and conductor placement can greatly enhance this effect. Our

experiments show that the E-field coupling depends slightly on the experimental conditions, is never higher than 15%–20% the maximum measured sensor output, and does not change the results presented in this article in any significant way. In the future, a fully differential architecture of the electrooptical transmitter would be desirable to overcome this limitation. We are also studying different designs of the toroidal sensor that may further reduce (or enhance) its sensitivity to RF electric field interference. Finally, future implementations may benefit from the use of a photonic power delivery system, such as those manufactured by JDS Uniphase Corporation. Photonic power distributes the laser-generated supply power via fiber optics and is thus virtually immune to any electromagnetic inference as well as to the static and time-varying magnetic fields of MRI.

## VI. CONCLUSION

In conclusion, we have designed, built and validated a low-cost, optically coupled system to measure the variations in the wire current induced by the RF field of an MRI scan, as confirmed by simultaneous measurement of the wire heating and by the laws of electromagnetics. We have also demonstrated simple and effective devices and methods to reduce the RF current and, thus, heating. Further work will focus on minimizing residual electromagnetic pickup. Since our system monitors induced currents associated with heating, and can detect the effectiveness of devices intended to reduce heating, it is a simple but important tool for safer use of MRI in the presence of long conductors, and is beneficial in a number of applications including but not limited to interventional MRI procedures.

## ACKNOWLEDGMENT

The authors would like to thank S. Smith, K. Edmunds, and K. Larson of Boston Scientific for the construction of the birdcage test platform.

## REFERENCES

- [1] J. A. Nyenhuis, P. Sung-Min, R. Kamondetdacha, A. Amjad, F. G. Shellock, and A. R. Rezaei, "MRI and implanted medical devices: Basic interactions with an emphasis on heating," *IEEE Trans. Dev. Mater. Rel.*, vol. 5, no. 3, pp. 467–479, Sep. 2005.
- [2] E. Kanal, A. J. Barkovich, C. Bell, J. P. Borgstede, W. G. Bradley, Jr, J. W. Froelich, T. Gilk, J. R. Gimbel, J. Gosbee, and E. Kuhni-Kaminski, "ACR guidance document for safe MR practices: 2007," *Am. J. Roentgenol.*, vol. 188-6, pp. 1447–1474, 2007.
- [3] M. F. Demspey, B. Condon, and D. M. Hadley, "Thermal injuries associated with MRI," *Clin. Radiol.*, vol. 56, pp. 457–465, 2001.
- [4] J. P. De Wilde, D. Grainger, D. L. Price, and C. Renaud, "Magnetic resonance imaging safety issues including an analysis of recorded incidents within the UK," *Progr. Nucl. Magn. Reson. Spectrosc.*, vol. 51, pp. 37–48, 2007.
- [5] J. L. Helfer, R. W. Gray, S. G. MacDonald, and T. W. Bibens, "Can pacemakers, neurostimulators, leads, or guide wires be MRI safe? Technological concerns and possible resolutions," *Minimally Invasive Therapy Allied Technol.*, vol. 15-2, pp. 114–120, 2006.
- [6] R. W. Gray, W. T. Bibens, and F. G. Shellock, "Simple design changes to wires to substantially reduce MRI-induced heating at 1.5 T: Implications for implanted leads," *Magn. Reson. Imag.*, vol. 23, pp. 887–891, 2005.
- [7] M. K. Konings, L. W. Bartels, H. F. Smits, and C. J. Bakker, "Heating around intravascular guidewires by resonating RF waves," *J. Magn. Res. Imag.*, vol. 12, pp. 79–85, 2000.
- [8] C. Armenean, E. Perrin, M. Armenean, O. Beuf, Olivier, F. Pilleul, and H. Saint-Jalmes, "RF-induced temperature elevation along metallic wires in clinical magnetic resonance imaging: Influence of diameter and length," *Magn. Reson. Med.*, vol. 52, pp. 1200–1206, 2004.

- [9] S. M. Park, R. Kamondetdacha, A. Amjad, and J. A. Nyenhuis, "MRI safety: RF-induced heating near straight wires," in *IEEE Trans. Magn.*, 2005, vol. 41, no. 10, pp. 4197–4199.
- [10] W. R. Nitz, A. Oppelt, W. Renz, C. Manke, M. Lenhart, and J. Link, "On the heating of linear conductive structures as guide wires and catheters in interventional MRI," *J. Magn. Reson. Imag.*, vol. 13, pp. 105–114, 2001.
- [11] R. W. P. King, "The many faces of the insulated antenna," *Proc. IEEE*, vol. 64, pp. 228–238, Feb. 1976.
- [12] R. W. P. King, "Embedded bare and insulated antennas," *IEEE Trans. Biomed. Eng.*, vol. BME-24, no. 3, pp. 253–260, May 1977.
- [13] R. W. P. King, B. Sandler, and T. T. Wu, "Cylindrical antennas immersed in arbitrary homogeneous isotropic media," *J. Appl. Phys.*, vol. 40, pp. 5049–5065, 1969.
- [14] R. W. P. King, C. Harrison, Jr., and D. Tingley, "The current in bare circular antennas in a dissipative medium," *IEEE Trans. Antennas Propag.*, vol. 13, no. 4, pp. 529–551, Jul. 1965.
- [15] R. W. P. King and S. Prasad, *Fundamental Electromagnetic Theory and Applications*. Englewood Cliffs, NJ: Prentice-Hall, 1986.
- [16] R. King and L. Scott, "The cylindrical antenna as a probe for studying the electrical properties of media," *IEEE Trans. Antennas Propag.*, vol. 19, no. 3, pp. 406–416, May 1971.
- [17] R. Venook, W. Overall, J. Pauly, and C. G. Scott, "Reducing and monitoring resonant heating in MR guidewires," in *Proc. 14th ISMRM*, 2006, p. 2037.
- [18] M. E. Ladd, "Reduction of resonant RF heating in intravascular catheters using coaxial chokes," *Magn. Res. Med.*, vol. 43, pp. 615–619, 2000.
- [19] C. M. Hillenbrand, D. R. Elgort, E. Y. Wong, A. Reykowski, F. K. Wacker, J. S. Lewin, and J. L. Duerk, "The bazooka coil: A novel dual-purpose device for active visualization and reduction of cable currents in electrically conductive endovascular instruments," in *Proc. 13th ISMRM*, 2005, p. 197.
- [20] H. Bassen, M. Swicord, and J. Abita, "A miniature broad-band electric field probe," *Ann. NY Acad. Sci.*, vol. 247, pp. 481–493, 1975.
- [21] G. S. Smith, "The electric-field probe near a material interface with application to the probing of fields in biological bodies," *IEEE Trans. Microw. Theory Tech.*, vol. 27, no. 3, pp. 270–278, Mar. 1979.
- [22] H. Bassen and G. Smith, "Electric field probes—A review," *IEEE Trans. Antennas Propag.*, vol. 31, pp. 710–718, Sep. 1983.
- [23] H. C. Taylor, M. Burl, and J. W. Hand, "Design and calibration of electric field probes in the range 10–120 MHz," *Phys. Med. Biol.*, vol. 42-7, pp. 1387–1394, 1997.
- [24] S. Fandrey, S. Weiss, and J. Muller, "Development of an active intravascular MR-device with an optical transmission system," *Trans. Med. Imag.*, vol. 27, no. 12, pp. 1723–1727, Dec. 2008.
- [25] S. Weiss, H. Eggers, and T. Schaeffter, "MR-controlled fast optical switching of a resonant circuit mounted to the tip of a clinical catheter," in *Proc. 9th Int. Soc. Magn. Reson. Med.*, 2001, p. 554.
- [26] E. Mattei, G. Calcagnini, M. Triventi, F. Censi, P. Bartolini, W. Kainz, and H. Bassen, "MRI induced heating of pacemaker leads: Effect of temperature probe positioning and pacemaker placement on lead tip heating and local SAR," in *Proc. Eng. Med. Biol. Soc.*, 2006, vol. 1, p. 1889.
- [27] P. Nordbeck, F. Fidler, I. Weiss, M. Warmuth, M. T. Friedrich, P. Ehse, W. Geisert, O. Ritter, P. M. Jakob, and M. E. Ladd, "Spatial distribution of RF-induced E-fields and implant heating in MRI," *Magn. Reson. Med.*, vol. 60, no. 2, pp. 312–319, 2008.
- [28] P. Nordbeck, I. Weiss, P. Ehse, O. Ritter, M. Warmuth, F. Fidler, V. Herold, P. M. Jakob, M. E. Ladd, and H. H. Quick, "Measuring RF-induced currents inside implants: Impact of device configuration on MRI safety of cardiac pacemaker leads," *Magn. Reson. Med.*, vol. 61, no. 3, pp. 570–578, 2009.
- [29] S. M. Park, J. A. Nyenhuis, C. D. Smith, E. J. Lim, K. S. Foster, K. B. Baker, G. Hrdlicka, A. R. Rezai, P. Ruggieri, A. Sharan, F. G. Shellock, P. H. Stypulkowski, and J. Tkach, "Gelled versus nongelled phantom material for measurement of MRI-induced temperature increases with bioimplants," *IEEE Trans. Magn.*, vol. 39, no. 9, pp. 3367–3371, Sep. 2003.
- [30] R. Venook, W. Overall, S. Conolly, J. Pauly, and C. G. Scott, "Artifact-based measurement of induced currents on long conductive structures during MRI," in *Proc. MR Safety: Update, ISMRM Workshop Series*, 2008.
- [31] W. Overall, P. Stang, J. Pauly, and C. G. Scott, "Detecting unsafe device coupling using reversed RF polarization," in *Proc. 17th ISMRM*, 2009, p. 305.